RSC Advances

PAPER

View Article Online
View Journal | View Issue

Check for updates

Cite this: *RSC Adv.*, 2022, **12**, 12160

Novel poly(epichlorohydrin)-based matrix for monolithic ionogel electrolyte membrane with high lithium storage performances

Chunming Chen, [a] Qiong Chen,[a] Jian Xie [*ab] and Zhonghua Chen*[c]

Based on gelling matrices and ionic liquids (ILs), monolithic ionogel electrolyte membranes (MIEMs) have become a research focus. However, further application is limited by lack of functional matrices. Herein, we proposed the introduction of an ionized polymer, *i.e.*, polyether polymer with side-chain ionic groups obtained *via* the reaction of quaternary ammonium with uncrystallizable poly (epichlorohydrin) (PECH), as the matrix into the gels to balance the mechanical properties and the ionic conductivity. In combination with lithium bis-(fluorosulfonyl) imide (LiFSI) and 1-ethyl-3-methylimidazolium bis-(fluorosulfonyl)-imide (EMImFSI) *via* a solvent casting technique, a flexible MIEM was successfully prepared. The as-obtained MIEM exhibited good thermal stability (up to about 250 °C) and a high ionic conductivity of 1.21 mS cm^{-1} at 20 °C. Moreover, Li|$LiFePO_4$ coin cells using this MIEM delivered high capacity (150.0 mA h g^{-1} at 0.2C) with good cycling stability, and an excellent C-rate response. This work discloses a novel and paramount route to exploit PECH-based MIEMs for Li storage, as well as energy storage systems beyond Li.

Received 7th January 2022
Accepted 13th April 2022

DOI: 10.1039/d2ra00110a

rsc.li/rsc-advances

Open Access Article. Published on 21 April 2022. Downloaded on 1/15/2026 12:07:17 AM.
This article is licensed under a Creative Commons Attribution-NonCommercial 3.0 Unported Licence.

Introduction

Due to their high specific energy and long cycle life, lithium ion batteries (LIBs) have been widely used as the main power sources in energy storage and electric vehicles (EVs).[1–3] However, current commercial LIBs still using flammable organic solvents as the electrolyte components have unavoidable drawbacks such as flammability and leakage, which limit their further development, especially in flexible and wearable devices.[4,5] In order to overcome these safety limitations, continual research efforts have been carried out for decades. Polymer-based electrolytes have been widely studied since Fenton *et al.*[6] first reported them in 1973. Although most polymer electrolytes obtained *via* complexation of poly(ethylene oxide) (PEO) with alkali metal salts present ionic conductivity, their ionic conductivity still cannot meet the requirements for actual applications in LIBs.[7–10] Alternatively, gel polymer electrolytes (GPEs) developed in 1995, which consist of a gel polymer network formed by polymers, plasticizers, and lithium salts, have flexibility and comparatively high ionic conductivity originating from the liquid electrolyte molecules fixed in the microstructures.[11–14] With polar functional groups, typical polymers, *e.g.*, PEO, poly (acrylonitrile) (PAN), poly(methyl methacrylate) (PMMA), and poly(vinylidene fluoride) (PVDF),[15,16] have been used as the matrices to prepare GPEs. Among them, PEO is of particular interest. This can be ascribed to its ability to easily form complexes with lithium salts, high mobility of charge carriers, and stable chemical properties.[17] Note that lithium salts are the main source of charge carriers in PEO-based GPEs. As Li ions could coordinate with oxygen atoms in PEO, charge carriers could easily move in these systems.[18] However, high degree of crystallinity of PEO is very unfavorable for ion transport. In addition, crystalline areas of polymer matrix are disadvantageous for gelation processes, resulting in inferior ionic transport.[19] Therefore, much effort has been devoted to inhibiting the crystallinity and improving the movement ability of the PEO chains.[20] Also, another effective way is to introduce cross-linked bonds into host polymer structures to form grafting copolymers, block copolymers, cross-linked networks, polymer blends, *etc.*[21–29] The conductivity of the polymer electrolytes depends on the properties of lithium salt and organic plasticizer as well as polymer matrixes. Owing to high ionic conductivity, excellent electrochemical properties and remarkable thermal stability, ionic liquids (ILs) have been used as the organic plasticizers.[30] ILs not only act as plasticizers but also charge carriers in polymer electrolytes; therefore, the conductivity of GPEs featuring ILs as the plasticizers is much higher than the counterparts using organic solvents as plasticizers. Furthermore, GPEs featuring ILs present good flexibility and compatibility with electrode interfaces.[31] Numerous types of GPE matrices have been reported to date, including

[a]*School of Chemistry and Environmental Engineering, Hanshan Normal University, Chaozhou 521041, China. E-mail: xiejian@hstc.edu.cn*

[b]*Hunan Provincial Key Laboratory of Water Treatment Functional Materials, Hunan University of Arts and Science, Changde, 415000, China*

[c]*College of Materials Science and Engineering, South China University of Technology, Guangzhou 510640, China. E-mail: cezhchen@scut.edu.cn*

© 2022 The Author(s). Published by the Royal Society of Chemistry

Open Access Article. Published on 21 April 2022. Downloaded on 1/15/2026 12:07:17 AM.
This article is licensed under a Creative Commons Attribution-NonCommercial 3.0 Unported Licence.

inorganic, linear polymer (such as PEO), block copolymer, and the hybrid matrices.[32–35] However, the electroneutrality of the polymer matrixes leads to weak interactions between the polymer and the IL, which are harmful to the increase in ionic conductance of the GPEs, and could also easily cause the phase separation inside the gels. In general, introducing a poly (ionic liquid) (PIL) into the GPEs could enhance the ion–ion interactions, but the mechanical properties and ionic conductivity of the GPEs are often affected in the processes.[36]

It is well known that the poly (epichlorohydrin) (PECH) is an uncrystallizable rubber with excellent resistance to ozone, heat, oil, and weathering. It is also very flexible owing to the presence of polyether groups in its structure. Herein, we proposed the introduction of an ionized polymer, *i.e.*, the polyether polymer with the side-chain ionic groups obtained *via* the reaction of quaternary ammonium with poly (epichlorohydrin) (PECH), as the matrix into gels to balance mechanical properties and ionic conductivity of the gel. Due to the main chain containing ether ($-CH_2-CH_2-O-$) units and the side chains containing ionic moieties, the obtained quaternary ammonium poly (epichlorohydrin) (PECH) presented the properties of both polyether and PIL. In combination with the lithium bis-(fluorosulfonyl) imide (LiFSI) and the 1-ethyl-3-methylimidazolium bis-(fluorosulfonyl)-imide (EMImFSI) *via* the solvent casting technique, flexible monolithic ionogel electrolyte membrane (MIEM) with high thermal stability and a high ionic conductivity of 1.21 mS cm^{-1} at 20 °C was successfully prepared. Furthermore, Li|$LiFePO_4$ cells with the unique MIEM at 0.2C exhibited a discharge capacity of 150.0 mA h g^{-1}, with high cycling stability and rate performances (125.8 mA h g^{-1} at 1C).

Experimental

Preparation of quaternary ammonium poly (epichlorohydrin) (PECH) with the side chain of the bis-(fluorosulfonyl) imide (QAPECHFSI)

PECH rubber (Daiso Co., Ltd., Japan) with chlorine content of 37 wt%, weight-average molecular weight of 700 000 and density of 1.36 g cm^{-3}, was used as the quaternary ammonium polymer matrix. Quaternary ammonium PECH was synthesized in a 50 mL three-necked flask equipped with a reflux condenser and Teflon stirrer. First, PECH (1 g) and methyl ethyl ketone (MEK, 10 g) were added to the flask and the mixture was stirred until a transparent solution was formed; then hexadecyl trimethyl ammonium bromide (HTAB, 0.01 g, Sigma-Aldrich) and *N*-methyl imidazole (5 g) were added to the solution, and stirring was continued at 75 °C for 48 h. The viscous liquid obtained was washed three times with diethyl ether (DEE) and subsequently dried in vacuum for 6 h to obtain quaternary ammonium poly (epichlorohydrin) (QAPECH) precursor. Then, the precursor (1 g) was added to dimethylsulfoxide (DMSO, 20 mL, Sigma-Aldrich), and the mixture was vigorously stirred at ambient temperature. Afterward, lithium bis-(fluorosulfonyl) imide (LiFSI, 10 wt%, 30 mL, Sigma-Aldrich) aqueous solution was dropwise added to initiate the anion exchange reaction, and stirring was continued for 2 h. Subsequently, the solution was precipitated with the deionized water. The as-obtained precipitate was further washed with ethanol at least three times to remove the chloride and then dried in oven at 60 °C to constant weight. Finally, the QAPECH with the side chain of bis-(fluorosulfonyl) imide (QAPECHFSI) was achieved.

Preparation of the monolithic ionogel electrolyte membrane (MIEM)

Firstly, the as-prepared QAPECHFSI, commercially available 1-ethyl-3-methylimidazolium bis-(fluorosulfonyl)-imide (EMImFSI) and the LiFSI were dried at 60 °C for 4 h. Using the *N*,*N*-dimethylformamide (DMF, Sigma-Aldrich) as the solvent, the monolithic ionogel electrolyte membrane (MIEM) was prepared *via* the solvent casting technique. Typically, a mixture of the QAPECHFSI, LiFSI and EMImFSI in a weight ratio of 6 : 2 : 2 was dissolved in DMF at room temperature. Then the polymer salt complex was stirred well for 24 h, degassed to remove air bubbles, poured on a polytetrafluoroethylene (PTFE) sheet, and dried under vacuum at 80 °C for 24 h to obtain free-standing films, which subsequently were harvested and stored in highly evacuated desiccators to prevent from absorbing moisture. Approximately 170 μm-thick flexible thin films with the PTFE sheet support were thus obtained. Finally, the as-achieved MIEMs were punched into a round disk with a diameter of 19 mm for later use.

Characterizations

The structure and the chemical composition of the materials were analyzed using an IRAffinity-1 (Shimadzu, Japan) Fourier-transform infrared (FTIR) spectrometer operated in the wavenumber range of 4000–500 cm^{-1}, and was further determined by the ^1H nuclear magnetic resonance (NMR). Differential scanning calorimeter (DSC, 204F1, NETZSCH) was employed to investigate the thermal behavior of the samples between −70 and 150 °C under a nitrogen atmosphere at a rate of 10 °C min^{-1}. The thermal stability was tested *via* the thermogravimetric analyses (TGA, STA409, NETZSCH) from 20 to 500 °C under a nitrogen atmosphere at a heating rate of 20 °C min^{-1}. The mechanical properties were measured using a WDW-100Y (Shanghai, China) universal testing machine at room temperature.

Ionic conductivities were measured *via* the AC impedance analysis in the range of 0.1 to 10^6 Hz on a CHI 660E (Chenhua, Shanghai) electrochemical workstation, using coin cells with MIEMs sandwiched between stainless steel (SS) blocking electrodes. The ionic conductivity (σ) was calculated based on the following equation: $\sigma = D/(RS)$, where D, S, and R are the thickness, surface area, and bulk resistance of the membrane, respectively.

Using CHI 660E electrochemical workstation, electrochemical stability of the obtained MIEM was further investigated at room temperature by linear sweep voltammetry (LSV) assembling the CR2016 cell, with the stainless steel as the working electrode and lithium metal foil as the reference and counter electrode. The potential ranged from 2.5 to 6.0 V at 1 mV s^{-1}.

Open Access Article. Published on 21 April 2022. Downloaded on 1/15/2026 12:07:17 AM.
This article is licensed under a Creative Commons Attribution-NonCommercial 3.0 Unported Licence.

In order to further investigate electrochemical performances of MIEMs, CR2016 coin cells, Li/MIEM/$LiFePO_4$, were assembled in an Ar-filled glove box with the O_2 and the H_2O < 1 ppm. Using the MIEM as the polymer electrolyte, the MIEM sandwiched between the $LiFePO_4$ cathode and the lithium anode and sealed in CR2016 coin cell. Such cell assembling processes are the same to the counterparts as reported in the literature.[37,38] The discharge/charge measurements were conducted in the voltage window of 2.6–4.2 V on a Land CT2001A battery test system. Li foils were employed as the reference and counter electrode. The cathode consisted of commercial $LiFePO_4$, super P and PVDF (in an 8 : 1 : 1 weight ratio, respectively) was prepared by the doctor blade method on an Al foil and dried at 110 °C in vacuum for 12 h to remove the remaining *N*-methylpyrrolidinone (NMP) solvent, and then roll pressed to enhance particulate contact and adhesion to the current collector. After further drying, the cathode was punched into round disks of 12 mm in diameter. The average mass loading of $LiFePO_4$ for the electrode was typically 1.5–2.0 mg cm^{-2}, similar to the value (1.0–2.0 mg cm^{-2}) as reported in relative literature.[37–39]

Results and discussion

Scheme 1 shows the schematic synthesis route of QAPECHFSI and MIEM. As depicted in Scheme 1, the achieved quaternary ammonium poly (epichlorohydrin) (QAPECH) precursor was obtained *via* the reaction of *N*-methyl imidazole with PECH. Then, QAPECH with the side chain of bis-(fluorosulfonyl) imide (QAPECHFSI), the matrix for MIEMs, was achieved by the anion reaction with the LiFSI. In combination with EMImFSI and LiFSI, flexible MIEM was prepared *via* solvent casting technique. In general, as the quaternization degree of PECH increased, ionic conductivity and tensile strength increased and decreased, respectively. To balance such opposite trends of the mechanical properties and ionic conductivity, the quaternization reaction time was set at 48 h, and the obtained QAPECHFSI membrane presented a high ionic conductivity of 4.57 mS cm^{-1}. Also, it is mechanically robust, with the yield stress of over 2.0 MPa and elongation at break of 205% at room temperature at a pull rate of 200 mm min^{-1}.

FTIR spectra of PECH and QAPECHFSI are shown in Fig. 1A. The strong absorption peaks at 2957, 2920, and 2876 cm^{-1} correspond to the stretching vibrations of aliphatic C–H groups in PECH. The peak at 1100 cm^{-1} is attributed to the stretching vibrations of the C–O–C bonds, while the moderately strong peak at 1431 cm^{-1} is assigned to bending vibrations of the asymmetric and symmetric C–H bonds. The absorption peak at 1265 cm^{-1} is ascribed to the stretching vibrations of C–H bonds of the $-CH_2Cl$ groups in PECH, and the peak at 743 cm^{-1} is attributed to the stretching vibrations of C–Cl bonds of $-CH_2Cl$ groups. In addition, the absorption peaks at approximately 3387 and 3111 cm^{-1} in the FTIR spectrum of QAPECHFSI could be attributed to the stretching vibrations of C–H bonds of the *N*-methylimidazole moieties, which confirm formation of quaternary ammonium compound. The moderately strong peak at 2360 cm^{-1} is ascribed to the imidazole ring of *N*-methylimidazole, and the moderately strong absorption peak at 1516 cm^{-1} is attributed to C–N bonds of the *N*-methylimidazole. Note that the absorption band at 743 cm^{-1} belonging to the stretching vibrations of C–Cl bonds nearly disappears in the obtained QAPECHFSI, which implies that most chloromethyl groups reacted during the quaternization reaction. To further validate imidazole group was successfully attached, the structure of QAPECHFSI was measured by nuclear magnetic resonance (^1H NMR). As shown in Fig. 1B, the chemical shifts at 6.8–7.7 ppm indicate the existence of the imidazole ring, while the one at 3.6 ppm is assigned to the methyl on the imidazole ring. Those at 3.4–3.7 ppm are the signal of the previous methyl and methylene.

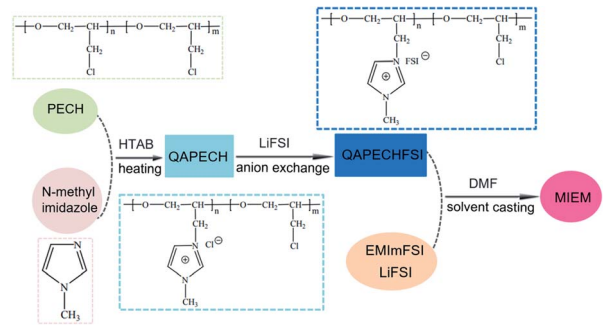

Scheme 1 Schematic diagram for the preparation of the quaternary ammonium poly (epichlorohydrin) with the bis-(fluorosulfonyl) imide side chain (QAPECHFSI) and resulted monolithic ionogel electrolyte membrane (MIEM) (HTAB: hexadecyl trimethyl ammonium bromide; LiFSI: lithium bis (fluorosulfonyl)imide; EMImFSI: 1-ethyl-3-methylimidazolium bis-(fluorosulfonyl)-imide; DMF: *N*,*N*-dimethylformamide).

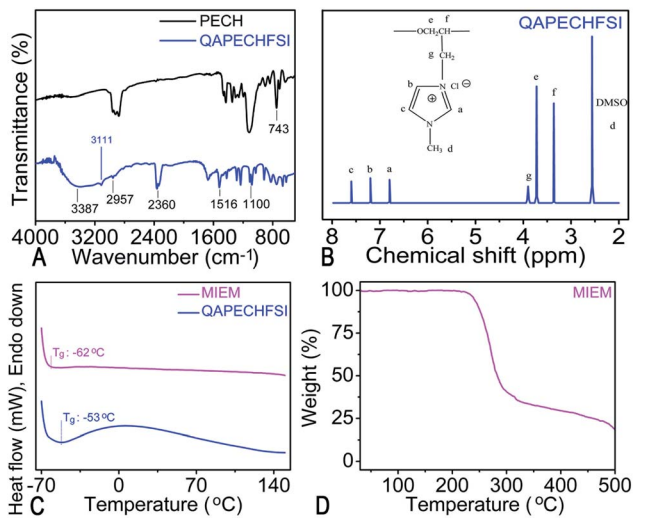

Fig. 1 (A) Fourier-transform infrared (FTIR) spectra of the poly (epichlorohydrin) (PECH) and the quaternary ammonium poly (epichlorohydrin) with side chain of bis-(fluorosulfonyl) imide (QAPECHFSI); (B) ^1H NMR spectrum of the QAPECHFSI; (C) differential scanning calorimeter (DSC) curves of QAPECHFSI and the monolithic ionogel electrolyte membrane (MIEM); (D) thermogravimetric analysis (TGA) curves of MIEM.

© 2022 The Author(s). Published by the Royal Society of Chemistry

Open Access Article. Published on 21 April 2022. Downloaded on 1/15/2026 12:07:17 AM.
This article is licensed under a Creative Commons Attribution-NonCommercial 3.0 Unported Licence.

Differential scanning calorimetry (DSC) was used to study the phase transition process. As shown in Fig. 1C, the endothermic peaks located at −53 °C could be assigned to the glass transition temperature (T_g) of the QAPECHFSI. When EMImFSI was added into the framework of the QAPECHFSI, the T_g value of the whole electrolyte system, MIEM, is significantly reduced to −62 °C, and no melting peaks could be found in the temperature range of the measurement. It is concluded that it does not occur phase separation between the lithium salt and the IL since EMImFSI plays a plasticizer role in the polymer electrolyte system. On one hand, it increases the distance between molecular chains of QAPECHFSI polymer; and on the other hand, it is equivalent to coating the QAPECHFSI with the lubricant, thus weakening the movement resistance of the QAPECHFSI polymer segment.[40] Note that lower T_g would lead to the higher ionic conductivity.[41]

Thermal stability is an important indicator for evaluating the safety performance. As the TGA curve shown in Fig. 1D, the resulted MIEM exhibits stability up to 250 °C, much higher than that reported in the most recent literature.[42] It reveals that no phase transition peaks exist until decomposition temperature, further implying the presence of an amorphous phase in the structure of MIEM. This could be attributed to the interactions between the polymer chains and ions, which inhibit possible crystallization processes. The segmental flexibility and lower fraction of crystalline phase of the MIEM could contribute to a high ionic conductivity. Moreover, the above thermal stability results suggest that the MIEM is very promising to construct safe and thermally stable LIBs.

As shown in Scheme 1, MIEM was prepared by mixing the QAPECHFSI, LiFSI, and EMImFSI. Of these, QAPECHFSI was used as the polymer matrix to provide the required mechanical properties for the MIEM, while the EMImFSI was used as the plasticizer, and it was combined with LiFSI to confer good ionic conductivity to the MIEM. In this study, we fixed mass fraction of the LiFSI and the EMImFSI in the electrolyte system on 20 and 15 wt%, respectively.

The conductivity of the MIEM is an important parameter, which is closely related to the performance of LIBs. After the MIEM was prepared, the ionic conductivity was measured at different temperatures using impedance spectroscopy. Fig. 2A presents the temperature dependence of ionic conductivities of the achieved MIEM. The ionic conductivity depends largely on temperature and increases significantly as the temperature increases from 20 to 70 °C. The MIEMs exhibit high ionic conductivities of 1.21 and 4.49 mS cm^{-1} at 20 and 70 °C, respectively, higher than those of the counterparts as reported in literatures.[5,42–47] This trend could be ascribed to the increase in the flexibility of the MIEM and faster diffusion of the ions with increasing temperatures. The ionic conductivity of LIBs should exceed 0.1 mS cm^{-1} in the working temperature ranges of 20–70 °C, and the MIEM prepared herein fulfilled this requirement.

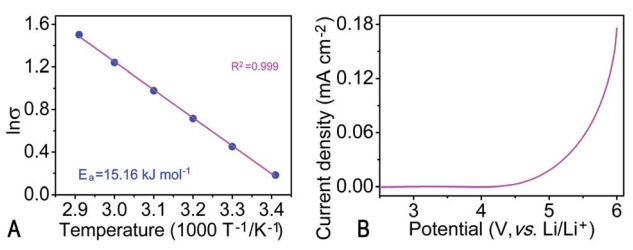

Fig. 2 (A) ln σ dependence on temperature (T) of the resulted monolithic ionogel electrolyte membrane (MIEM) (ln σ *vs.* T^{-1} plot); (B) linear sweep voltammograms (LSV) of the MIEM.

The ln σ *vs.* 1000 T^{-1} plot of the MIEM is depicted in Fig. 2A and is almost linear in the wide temperature range of 20–70 °C. The temperature (T) dependence of the ionic conductivity (σ) can be described using the Arrhenius equation: $\sigma = A\exp(-E_a/RT)$; where A is a constant, E_a is the activation energy, and R is the gas constant (8.314 J K^{-1} mol^{-1}). The activation energy of ionic conductivity could be estimated using the slope of the curve as follows: $E_a = -\text{slope} \times R$. The E_a values of the MIEM is 15.16 kJ mol^{-1}, implying that the MIEM has plenty transfer channels to facilitate the movement of the ions. The ionic conductivity of the polymer electrolytes is closely related to the mobility of the polymer segments. Although the addition of the EMImFSI would decrease the mechanical properties owing to the plasticity of the EMImFSI, we still obtain the MIEM with suitable mechanical properties. In addition, the as-synthesized MIEM was flexible, which is useful for assembling non-flat shaped batteries for the wearable devices. LSV was carried out at a scan rate of 1 mV s^{-1} to examine the electrochemical stability of the MIEM, as shown in Fig. 2B. The anodic limit of the MIEM is evaluated to be about 5 V (*vs.* Li/Li$^+$), which indicates good electrochemical stability. This is similar to that of the PEO–P_{12}FSI–LiFSI solid polymer electrolyte (5.3 V).[37] Owing to the above-mentioned favorable properties, the as-prepared MIEM was assembled into Li/$LiFePO_4$ cells to further evaluate their potential applications (Fig. 3). As the 1st, 10th and 60th charge/discharge curves at 0.2C displayed in Fig. 3A, the charge/discharge voltage plateaus are all flat and remain almost unchanged with continued cycling and emerge at 3.5 and 3.4 V (*vs.* Li/Li$^+$), respectively, which is typical for Li/$LiFePO_4$ cells. The polarization voltage is less than 110 mV even at 60th cycle, much smaller than that reported recently,[46] implying fast Li ion transportation and electrochemical reaction kinetics in MIEM, which is consistent with the aforementioned LSV results.

The discharge capacity for the initial cycle is 139.6 mA h g^{-1}. Such a high capacity and excellent cycling performance achieved by the Li/MIEM/$LiFePO_4$ cells could be ascribed to the formation of the protective IMEM film on the electrode surface.

As illustrated in Fig. 3B, the discharge capacity slightly increases during the initial several cycles, probably owing to the optimization of the electrode/MIEM interface. The cell could deliver a discharge capacity of about 150.0 mA h g^{-1} (88.2% of the theoretical value) after 10 cycles and still maintain at 148 mA h^{-1} at the 60th cycle. In addition, the Coulombic efficiency (CE, Fig. 3C) of the cell reaches approximately 100% after several cycles.

Furthermore, rate capability was also checked. As depicted in Fig. 3D and E, discharge capacity reveals a typical step-like drop as the current rate increases. However, the polarization voltage

Open Access Article. Published on 21 April 2022. Downloaded on 1/15/2026 12:07:17 AM.
This article is licensed under a Creative Commons Attribution-NonCommercial 3.0 Unported Licence.

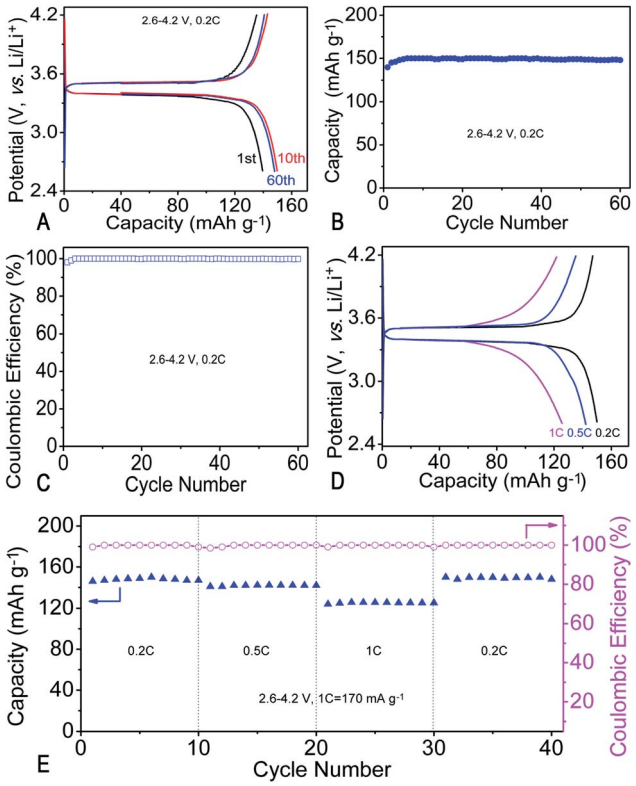

Fig. 3 Electrochemical performances of Li/MIEM/$LiFePO_4$ cells at 20 °C: (A) charge/discharge profiles for the 1st, 10th and 60th cycle, (B) discharge capacity and (C) Coulombic efficiency during cycling at 0.2C; (D) representative charge/discharge voltage profiles at current densities from 0.2C to 1C; (E) capacity and Coulombic efficiency during cycling at current densities from 0.2C to 1C (each for ten successive cycles).

is still less than 110 mV even at a high current density of 1C, further proving fast electrochemical reaction kinetics in MIEM (Fig. 3D). It is capable of reaching stable capacities of about 142.2 mA h g^{-1} (84% of the theoretical value) and 125.8 mA h g^{-1} (74% of the theoretical value) at 0.5C and 1C, respectively, for every ten successive cycles. When the current rate returns to 0.2C (Fig. 3E), the capacity is restored to the original value of 150.0 mA h g^{-1}, indicating much excellent and stable lithium storage performances at various current rates.

Conclusions

In summary, a novel flexible MIEM based on the uncrystallizable PECH is successfully prepared by combining the LiFSI and the EMImFSI into the QAPECHFSI matrix. The as-achieved MIEM presents attractive properties in terms of thermal stability, ionic conductivity and mechanical ability. We opt to examine their usability in LIBs and find that the unique MIEM structures yield high discharge capacities, remarkable cycling, and excellent rate performances. Overall, this work discloses a novel and essential route to exploit the ionogel polymer electrolyte membranes for next-generation all-solid-state lithium storage.

Conflicts of interest

There are no conflicts of interest to declare.

Acknowledgements

This work was financially supported by the Scientific Research Project of Department of Education of Guangdong Province (Grant No. 2020ZDZX2053, Grant No. 2020KQNCX045), Natural Science Foundation of Guangdong Province (Grant No. 2016A030307040), and National Natural Science Foundation of China (Grant No. 50973033). Also, Dr Jian Xie acknowledged for the financial support from the Open Funding Project of Hunan Provincial Key Laboratory of Water Treatment Functional Materials, Hunan University of Arts and Science in China (No. KFJJ2004).

Notes and references

1 J. M. Tarascon and M. Armand, *Nature*, 2001, **414**, 359–367.
2 J. Xie, L. Tong, L. Su, Y. Xu, L. Wang and Y. Wang, *J. Power Sources*, 2017, **342**, 529–536.
3 J. Xie, J. Carrasco, R. Li, H. Shen, Q. Chen and M. Yang, *J. Power Sources*, 2019, **431**, 226–231.
4 K. Xu, *Chem. Rev.*, 2014, **114**, 11503–11618.
5 J. Castillo, A. Santiago, X. Judez, I. Garbayo, J. A. Coca Clemente, M. C. Morant-Miñana, A. Villaverde, J. A. González-Marcos, H. Zhang, M. Armand and C. Li, *Chem. Mater.*, 2021, **33**, 8812–8821.
6 F. Wu, N. Chen, R. Chen, Q. Zhu, G. Tan and L. Li, *Adv. Sci.*, 2016, **3**, DOI: **10.1002/advs.201500306**.
7 B. Dunn, H. Kamath and J.-M. Tarascon, *Science*, 2011, **334**, 928–935.
8 V. Etacheri, R. Marom, R. Elazari, G. Salitra and D. Aurbach, *Energy Environ. Sci.*, 2011, **4**, 3243–3262.
9 J. B. Goodenough and Y. Kim, *Chem. Mater.*, 2010, **22**, 587–603.
10 D. E. Fenton, J. M. Parker and P. V. Wright, *Polymer*, 1973, **14**, 589.
11 J. B. Goodenough and K.-S. Park, *J. Am. Chem. Soc.*, 2013, **135**, 1167–1176.
12 X. Wang, H. Zhu, G. W. Greene, J. Li, N. Iranipour, C. Garnier, J. Fang, M. Armand, M. Forsyth, J. M. Pringle and P. C. Howlett, *J. Mater. Chem. A*, 2016, **4**, 9873–9880.
13 F. Makhlooghiazad, D. Gunzelmann, M. Hilder, D. R. MacFarlane, M. Armand, P. C. Howlett and M. Forsyth, *Adv. Energy Mater.*, 2017, **7**, DOI: **10.1002/aenm.201601272**.
14 N. Iranipour, D. J. Gunzelmann, A. Seeber, J. Vongsvivut, C. Doherty, F. Ponzio, L. A. O'Dell, A. F. Hollenkamp, M. Forsyth and P. C. Howlett, *J. Mater. Chem. A*, 2015, **3**, 6038–6052.
15 M. Forsyth, T. Chimdi, A. Seeber, D. Gunzelmann and P. C. Howlett, *J. Mater. Chem. A*, 2014, **2**, 3993–4003.
16 J. Y. Song, Y. Y. Wang and C. C. Wan, *J. Power Sources*, 1999, **77**, 183–197.

© 2022 The Author(s). Published by the Royal Society of Chemistry

Open Access Article. Published on 21 April 2022. Downloaded on 1/15/2026 12:07:17 AM.
This article is licensed under a Creative Commons Attribution-NonCommercial 3.0 Unported Licence.

17 W. Li, Y. Pang, J. Liu, G. Liu, Y. Wang and Y. Xia, *RSC Adv.*, 2017, **7**, 23494–23501.
18 L. Wu, R. I. Venkatanarayananan, X. Shi, D. Roy and S. Krishnan, *J. Mol. Liq.*, 2014, **198**, 398–408.
19 N. Kassenova, S. Kalybekkyzy, M. V. Kahraman, A. Mentbayeva and Z. Bakenov, *J. Power Sources*, 2022, **520**, DOI: **10.1016/j.jpowsour.2021.230896**.
20 J. G. Kim, B. Son, S. Mukherjee, N. Schuppert, A. Bates, O. Kwon, M. J. Choi, H. Y. Chung and S. Park, *J. Power Sources*, 2015, **282**, 299–322.
21 M. Y. Zhang, M. X. Li, Z. Chang, Y. F. Wang, J. Gao, Y. S. Zhu, Y. P. Wu and W. Huang, *Electrochim. Acta*, 2017, **245**, 752–759.
22 T. Zheng, Q. Zhou, Q. Li, L. Zhang, H. Li and Y. Lin, *Solid State Ionics*, 2014, **259**, 9–13.
23 H. Li, M. Li, S. H. Siyal, M. Zhu, J.-L. Lan, G. Sui, Y. Yu, W. Zhong and X. Yang, *J. Membr. Sci.*, 2018, **555**, 169–176.
24 Y. Kang, K. Cheong, K.-A. Noh, C. Lee and D.-Y. Seung, *J. Power Sources*, 2003, **119–121**, 432–437.
25 D. F. Miranda, C. Versek, M. T. Tuominen, T. P. Russell and J. J. Watkins, *Macromolecules*, 2013, **46**, 9313–9323.
26 S. H. Siyal, M. Li, H. Li, J.-L. Lan, Y. Yu and X. Yang, *Appl. Surf. Sci.*, 2019, **494**, 1119–1126.
27 Y. Shi, B. Li, Q. Zhu, K. Shen, W. Tang, Q. Xiang, W. Chen, C. Liu, J. Luo and S. Yang, *Adv. Energy Mater.*, 2020, **10**, DOI: **10.1002/aenm.201903534**.
28 Y. Zhou, X. Wang, H. Zhu, M. Armand, M. Forsyth, G. W. Greene, J. M. Pringle and P. C. Howlett, *Phys. Chem. Chem. Phys.*, 2017, **19**, 2225–2234.
29 Y. Zhou, X. Wang, H. Zhu, M. Yoshizawa-Fujita, Y. Miyachi, M. Armand, M. Forsyth, G. W. Greene, J. M. Pringle and P. C. Howlett, *ChemSusChem*, 2017, **10**, 3135–3145.
30 X. Liu, M. Zarrabeitia, A. Mariani, X. Gao, H. M. Schütz, S. Fang, T. Bizien, G. A. Elia and S. Passerini, *Small Methods*, 2021, **5**, DOI: **10.1002/smtd.202100168**.
31 M. Yoshizawa-Fujita, E. Kishi, M. Suematsu, T. Takekawa and M. Rikukawa, *Chem. Lett.*, 2014, **43**, 1909–1911.
32 L. Hu, Z. Tang and Z. Zhang, *J. Power Sources*, 2007, **166**, 226–232.
33 B. W. Zewde, S. Admassie, J. Zimmermann, C. S. Isfort, B. Scrosati and J. Hassoun, *ChemSusChem*, 2013, **6**, 1400–1405.
34 Z.-Y. Cui, Y.-Y. Xu, L.-P. Zhu, J.-Y. Wang, Z.-Y. Xi and B.-K. Zhu, *J. Membr. Sci.*, 2008, **325**, 957–963.
35 F. Wu, G. Tan, R. Chen, L. Li, J. Xiang and Y. Zheng, *Adv. Mater.*, 2011, **23**, 5081–5085.
36 X. Li, Z. Zhang, S. Li, K. Yang and L. Yang, *J. Mater. Chem. A*, 2017, **5**, 21362–21369.
37 S. Li, K. Yang, Z. Zhang, L. Yang and S.-i. Hirano, *Ind. Eng. Chem. Res.*, 2018, **57**, 13608–13614.
38 L. Liang, X. Chen, W. Yuan, H. Chen, H. Liao and Y. Zhang, *ACS Appl. Mater. Interfaces*, 2021, **13**, 25410–25420.
39 Z. Wang, H. Shi, W. Zheng, W. Sun, L. Zhao and W. Yuan, *J. Power Sources*, 2022, **524**, DOI: **10.1016/j.jpowsour.2022.231070**.
40 K. Yin, Z. Zhang, X. Li, L. Yang, K. Tachibana and S.-i. Hirano, *J. Mater. Chem. A*, 2015, **3**, 170–178.
41 D. G. Mackanic, X. Yan, Q. Zhang, N. Matsuhisa, Z. Yu, Y. Jiang, T. Manika, J. Lopez, H. Yan, K. Liu, X. Chen, Y. Cui and Z. Bao, *Nat. Commun.*, 2019, **10**, DOI: **10.1038/s41467-41019-13362-41464**.
42 F. Ahmed, D. Kim, J. Lei, T. Ryu, S. Yoon, W. Zhang, H. Lim, G. Jang, H. Jang and W. Kim, *ACS Appl. Mater. Interfaces*, 2021, **13**, 34102–34113.
43 L. Yu, L. Yu, Q. Liu, T. Meng, S. Wang and X. Hu, *Adv. Funct. Mater.*, 2022, **32**, DOI: **10.1002/adfm.202110653**.
44 J. Atik, J. H. Thienenkamp, G. Brunklaus, M. Winter and E. Paillard, *Electrochim. Acta*, 2021, **398**, DOI: **10.1016/j.electacta.2021.139333**.
45 Q. Sun, S. Wang, Y. Ma, Y. Zhou, D. Song, H. Zhang, X. Shi, C. Li and L. Zhang, *Energy Storage Materials*, 2022, **44**, 537–546.
46 G. Bai, N. Liu, C. Wang, W. Wei, X. Liu and Y. Li, *Chem. Commun.*, 2021, **57**, 11493–11496.
47 L. Liang, W. Yuan, X. Chen and H. Liao, *Chem. Eng. J.*, 2021, **421**, DOI: **10.1016/j.cej.2021.130000**.

© 2022 The Author(s). Published by the Royal Society of Chemistry